Characteristics of temporal fluctuations in the hyperpolarized state of the cortical slow oscillation

M. T. Wilson,[1,*] M. Barry,[2] J. N. J. Reynolds,[2] E. J. W. Hutchison,[1] and D. A. Steyn-Ross[1]
[1]*Department of Engineering, University of Waikato, Private Bag 3105, Hamilton 3240, New Zealand*
[2]*Department of Anatomy and Structural Biology, University of Otago School of Medical Sciences, P.O. Box 913, Dunedin 9016, New Zealand*

(Received 24 September 2007; revised manuscript received 21 February 2008; published 11 June 2008)

We present evidence for the hypothesis that transitions between the low- and high-firing states of the cortical slow oscillation correspond to neuronal phase transitions. By analyzing intracellular recordings of the membrane potential during the cortical slow oscillation in rats, we quantify the temporal fluctuations in power and the frequency centroid of the power spectrum in the period of time before "down" to "up" transitions. By taking appropriate averages over such events, we present these statistics as a function of time before transition. The results demonstrate an increase in fluctuation power and time scale broadly consistent with the slowing of systems close to phase transitions. The analysis is complicated and limited by the difficulty in identifying when transitions begin, and removing dc trends in membrane potential.

DOI: 10.1103/PhysRevE.77.061908 PACS number(s): 87.19.lj, 87.19.ln, 05.20.−y

I. INTRODUCTION

Recently, there have been many experimental quantifications of aspects of the cortical slow oscillation. During slow-wave sleep, the membrane potential of a cortical neuron cycles at a frequency of about 1 Hz between high-firing (or "up") states and low-firing (or "down") states [1,2]. These oscillations appear to be important for memory consolidation [3]. This can occur in small brain structures; for example, Rector *et al.* have used evoked potentials to demonstrate sleeplike states in individual cortical columns in the barrel cortex of rats [4]. However, the oscillation is also apparent across larger length scales; for example, Massimini *et al.* have mapped the propagation of waves of slow-wave activity across the cortex using a high-density electroencephalogram (EEG) [5]. Volgushev *et al.* have recently made intracellular recordings of the slow oscillation in several spatially separated neurons [6].

The mean-field approach provides an avenue for the modeling of large-scale assemblies of neurons [7–9]. As a result of such a treatment, Steyn-Ross *et al.* [10] have proposed that the cortex can have more than one stationary state—i.e., the model can have more than one equilibrium solution, and transitions between these states are analogous to first-order phase transitions. Recently, Wilson *et al.* have suggested that the oscillation between the low-firing and high-firing states in the cortical slow oscillation may be an example of this [11]. However, such descriptions in terms of phase transitions are still speculative—Bojak and Liley have successfully modeled the human EEG for anaesthetic induction without requiring their mean-field model to exhibit multiple stationary states [12], and Robinson *et al.* and Rennie *et al.* have described the major resonances of the EEG (including synchronous oscillations) by using linear analysis about a local solution to a mean-field thalamo-cortical model [13–15]. Moreover, Molaee-Ardekani *et al.* have recently reproduced the oscillation between up and down states with a model that does not have multiple stationary states [16].

We are therefore motivated to study intracellular recordings of the slow oscillation with the aim of identifying any evidence for or against the phase-transition explanation of the slow oscillation. The fact that this oscillation exists on many length scales (single neuron through to whole cortex) suggests that analysis of single-neuron recordings may in this case be reasonably compared to predictions from a mean-field modeling approach.

Computer simulations and theoretical analysis of a cortical mean-field model on the approach to a transition show an increase in temporal and spatial correlations [17]; therefore, experimental detection of such increased fluctuations would provide (nonconclusive) evidence for the hypothesis that the repeating down to up transitions of slow wave sleep can be described by first-order phase transitions. In order to measure spatial correlations, we require multiple simultaneous recordings from several neurons, and currently this is difficult (though Volgushev *et al.* report such a recording from four neocortical neurons [6].) However, it is possible to analyze the temporal fluctuations from a recording of the membrane potential from a single neuron. In this paper, we take a series of such recordings from neurons from the motor cortex of rats, and analyze the fluctuations in the membrane potential during the periods of time immediately preceding the transition from a down to an up state of the slow oscillation. Specifically, we look for evidence of an increase in the time scale of fluctuations, and an increase in fluctuation power, both of which would support the phase-transition hypothesis [18].

II. MATERIALS AND METHODS

All experiments were approved by the University of Otago Animal Ethics Committee (AEC 93/04).

A. Surgery

Male Wistar rats (280–390 g) were anesthetized with an intraperitoneal (IP) injection of urethane (1.6–2.0 g/kg body

*m.wilson@waikato.ac.nz

weight, Sigma-Aldrich, Inc., St. Louis, USA). The local anaesthetic bupivacaine (Astra-Zeneca, Australia) was applied to all incisions and pressure points, at a dose unlikely to produce any systemic effects (up to 2 mg/kg). Surgical anaesthesia was verified by the absence of the withdrawal reflex following administration of a toe pinch.

For intracellular recording, a craniotomy was performed over the left motor cortex (in relation to bregma: anteroposterior (AP); −1.0 to +4.0 mm, mediolateral (ML); +1.0 to +3.0 mm) and a burr hole was drilled in the skull for placement of a silver wire electrode against the dura, for EEG recording. The synchrony of the EEG wave form was used as an indication of depth of anaesthesia. Supplementary urethane (approximately 0.15 g/kg IP every 2 h) was administered on detecting EEG desynchronization. Dental acrylic was used to cement the EEG electrode in place and build a well around the craniotomy. During recording, the well was filled with paraffin wax to increase recording stability, and the cisterna magna was punctured to reduce brain pulsations.

B. Intracellular recording

Recording electrodes were sharp micropipettes (60–110 MΩ resistance) pulled from 3 mm glass capillaries, filled with 1*M* potassium acetate. These were lowered through the motor cortex in 1 μm steps using a Burleigh Inchworm micromanipulator (New York, USA) until a neuron was impaled or the maximum depth of 1.8 mm was reached. Recordings were made using an Axoclamp-900A amplifier digitized at 10 kHz with a Digidata 1322A and recorded using PCLAMP 10 software (Axon Instruments, Inc., California, USA).

The membrane potential activity of the recorded neuron was monitored continuously throughout the experiment until impalement was lost. Neurons were included in the study if they exhibited the following: (1) rhythmic membrane fluctuations between a relatively depolarized up state and a relatively hyperpolarized down state, with a down state membrane potential more negative than −60 mV; (2) fairly constant average membrane potential for the up and down states; and (3) action potentials that overshot 0 mV, with an amplitude greater than 50 mV. During the analysis of the results, a further criterion was applied, namely that the sequence had to exhibit at least 10 identifiable down to up transitions—this is a quantification of requirement (1) and the rationale is explained below. A total of nine sequences, each from a different rat, were selected in this way. Sequences were of at least 90 seconds and the sequences contained a total of 635 identified down to up transitions. Stable recording was continued for each neuron for at least 30 seconds after the end of the analyzed sequence, in most cases for at least several minutes following.

C. Neuronal classification

All neurons, bar one, were identified electrophysiologically as regular spiking pyramidal neurons, due to the characteristic train of single action potentials elicited in response to intracellular current injection [19,20]. The one neuron not tested with current injection was similar in other respects

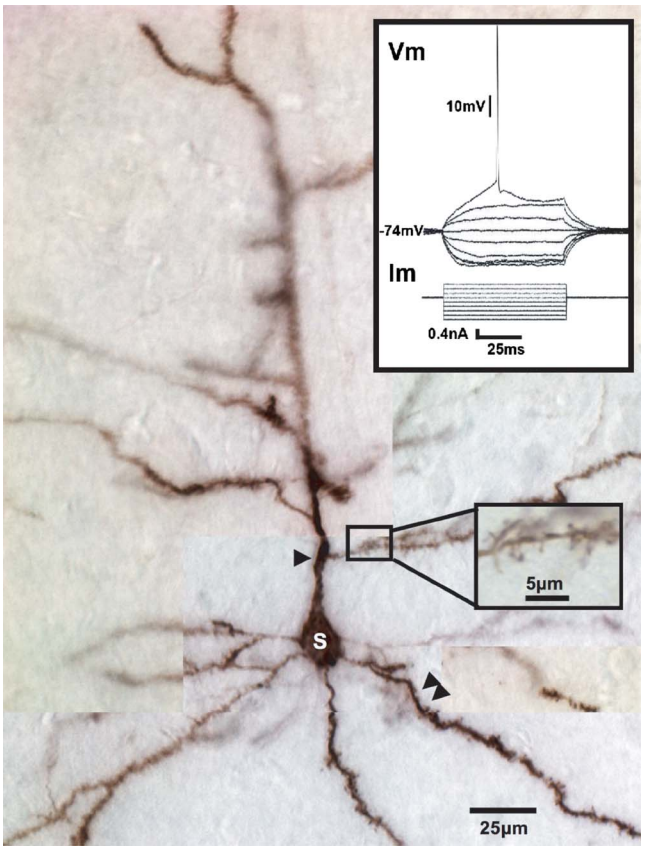

FIG. 1. (Color online) A cortical pyramidal neuron recorded intracellularly during the experiments from which the sample is taken. The basal dendrites (double arrowhead) arising from the pyramidal soma (*S*) are studded with dendritic spines, as are the oblique branches (enlarged inset) arising from the apical dendrite (arrowhead). The membrane potential ("Vm" in top inset) responds nonlinearly to negative current pulses ("Im") injected into the soma and fires a single action potential to a just-threshold positive current pulse.

electrophysiologically to the remainder of the sample. The depth of each neuron in the cortex was estimated by the travel of the pipette distance below the surface of the pia, as displayed on the Burleigh micromanipulator. Using an estimate for the interface between layer 3 and 5 in this region of approximately 600 μm [21,22], the sample comprises four neurons in layer 3 and five in layer 5. Neurons in each of these subgroups did not differ significantly in their firing frequencies, action potential parameters, or membrane potentials in the up or down states. In some experiments, 3% biocytin (Sigma) was included in the solution in the micropipette and the tissue processed after the experiment using established means [23] to identify the neuron. A representative example of a pyramidal neuron recorded during the series of experiments which yielded the sample is shown in Fig. 1. Due to technical limitations, we do not include the histology of a neuron used in the up and down state analysis presented here. However, the morphology and electrophysiology of the neuron shown is representative of all regular spiking pyramidal neurons we have recovered during our experiments.

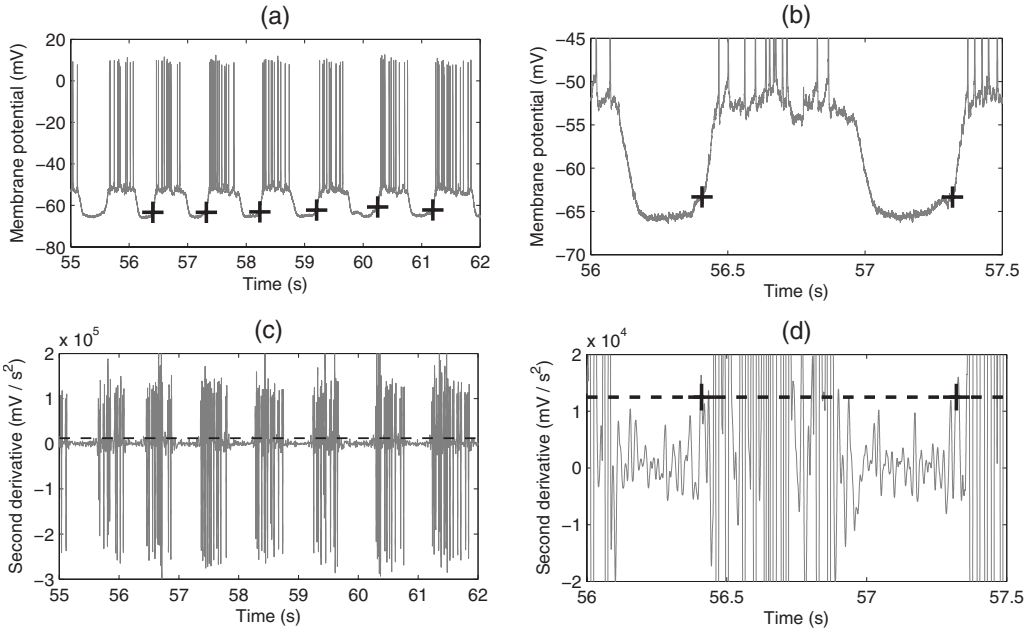

FIG. 2. (a) The membrane potential against time. The points of transition as identified by the threshold are marked with a "+" symbol. (b) A close-up view of two of the down-to-up transitions. (c) The second derivative of the membrane potential against time; the first-derivative being evaluated with a center-difference method based on 50 data points (or 0.005 s) forward and backward of the point of interest; the second-derivative using 100 data points (0.01 s) forward and backward. The extremely high values of the second derivative are due to action potentials, as can be seen from comparison with part (a). (d) A close-up view of the second derivative, for the same section of data as part (b). The threshold of 12 500 $\mathrm{mV/s^2}$ marked with a dashed line. The points of transition are indicated with the vertical bars. The second derivative must remain below the threshold for a period of more than 0.2 s for the upward crossing to be accepted as a transition.

III. ANALYSIS

We analyzed intracellular recordings of membrane potential against time. All recordings showed fluctuations in membrane potential between a down state and an up state, reflecting slow-wave oscillatory activity in corticothalamic networks due to urethane anaesthesia [1,20]. For the kth sequence ($k=1,\ldots,M$), where $M(=9)$ is the total number of sequences analyzed, we have a series of data points $y^k(j)$, where $j=1,\ldots,N^k$ with N^k being the total number of data points in the sequence. The "time" for each index j is equivalent to j/f_s, where f_s is the sample frequency (10 000 Hz).

First, we identify the locations of the down to up transitions. That is, for each sequence k, we want to locate the indices $j=T_i^k$ which correspond to the points where the sequence begins its ith transition from a down to an up state, with $i=1,\ldots,P^k$, where P^k is the total number of transitions in the kth sequence.

As can be seen in the example sequence in Fig. 2(a) the membrane potential begins to climb quickly as the down state ends and we use this fact to identify the point of transition (i.e., point in time where the membrane potential leaves the down state and starts a transition to the up state). We have done this by examining the second derivative of the membrane potential with respect to time—a high second derivative to corresponds to a rapid upward curve in membrane potential. A high curvature is a robust characteristic of the end of the down state. Although the transition from down to up also produces a large positive gradient (first derivative) the large variability in the shape of the transition means that the gradient may be largest at the end of the down state, at the start of the up state, or at any point in between. This makes a method based on the first derivative less reliable at identifying the point of transition where the down state ends. Specifically, we begin by defining the first time derivative at a point of interest with a center-difference method based on the mean over 50 data points before and after the point of interest; i.e., we define the derivative $d^{(1)k}(j)$ at the data point j as

$$d^{(1)k}(j)=\frac{f_s}{51}\left(\frac{1}{50}\sum_{l=1}^{50}y^k(j+l)-\frac{1}{50}\sum_{i=1}^{50}y^k(j-l)\right). \quad (3.1)$$

Using this result, we constructed the second time derivative $d^{(2)k}(j)$ for all data points in the sequence using a center-difference method based on the mean over 100 data points before and after the point of interest,

$$d^{(2)k}(j)=\frac{f_s}{101}\left(\frac{1}{100}\sum_{l=1}^{100}d^{(1)k}(j+l)-\frac{1}{100}\sum_{i=1}^{100}d^{(1)k}(j-l)\right). \quad (3.2)$$

We then applied a threshold of 12 500 $\mathrm{mV/s^2}$ to identify candidate transitions as the points when the second derivatives cross this threshold (going up). We only accept candidate transitions where the second derivative has remained below threshold for a period of 0.2 s before transition; this means that short down states and action potentials are excluded. This choice of method was selected because it gave a good performance in identifying down to up transitions. The

values for these parameters were chosen by systematically varying one parameter at a time, with a view to maximizing the classification rate of transitions while ensuring the algorithm had a virtually zero false-positive classification rate.

The method is summarized in Fig. 2. Part of a sequence is shown in Figs. 2(a) and 2(b), with the second derivative in Figs. 2(c) and 2(d). We mark the identified points of transition with a "+" symbol on (a) and (b). From an examination of all the sequences by eye it is clear that the method successfully located many transitions. Over the whole data set, only one automated classification was judged clearly incorrect on examination by eye; this was removed from the analysis.

We remark that identification of a particular time that corresponds to a transition is somewhat arbitrary; in practice the progression from a down to an up state takes around 0.1 s, and there is often no clear point at which we can say the down state ends. However, since we are primarily interested in the *changes* in the fluctuations on the approach to transition (specifically, whether they increase in power and time scale), exactly where we classify the transition is of less importance. We have also tried to implement the method of Volgushev *et al.* who found that they could identify up and down states from the statistics of the fluctuations in local field potential [6]; however, this did not prove as successful as the second derivative method described above.

We only present data for the down to up transitions, not the up to down transitions. This is because the up state is complicated by the presence of action potentials, which themselves are a limit cycle [18]. It would be a major undertaking to untangle voltage fluctuations due to the proximity to transition from those due to the preceding sequence of action potentials.

For each transition within a sequence we extract the membrane potentials for a period of 0.25 s *before* the transition. In other words, for the ith transition in the kth sequence, we define the data series

$$\tilde{y}^{ki}(j) = y^k(T_i^k - Q + j), \tag{3.3}$$

where $j=1,\ldots,Q$, with $Q=2500$ (i.e., 0.25 s $\times f_s$).

It is apparent from Fig. 3(a) that the average membrane potential of the neuron in the down state changes with time (it usually becomes less negative as it approaches the transition) and in order to analyze the spectrum of the fluctuations we must remove the average trend. This is not straightforward since we have no way of knowing *a priori* which changes in membrane potential are due to a change in average voltage, and which are due to low-frequency fluctuations [18], or even whether such a distinction can be made.

To proceed, for each sequence we construct the mean membrane potential over the 0.25 s preceding each transition, with the mean taken over all the identified down to up transitions in the sequence:

$$\bar{y}^k(j) = \frac{1}{P^k}\sum_{i=1}^{P^k} \tilde{y}^{ki}(j), \quad j=1,\ldots,Q. \tag{3.4}$$

By subtracting this mean trend from each of the 0.25 s segments of data, we can remove much of the overall trend in the neuron's membrane potential as it approaches the transition point, leaving the fluctuations about the trend. That is, we construct

$$\Delta\tilde{y}^{ki}(j) = \tilde{y}^{ki}(j) - \bar{y}^k(j), \quad j=1,\ldots,Q, \quad i=1,\ldots,P^k. \tag{3.5}$$

Figure 3(b) shows the mean potential $\bar{y}^{k=1}(j)$ in the time preceding the transition for the sequence shown in part in Fig. 3(a), and Fig. 3(c) shows some of the individual segments of data $\Delta\tilde{y}^{k=1,i}(j)$ once the mean trend has been subtracted. By inspection of Fig. 3(c), it can be seen that the subtraction of the mean membrane potential has not been entirely successful in removing the trend, and this issue is discussed further below. Removal of the trend necessarily removes low fre-

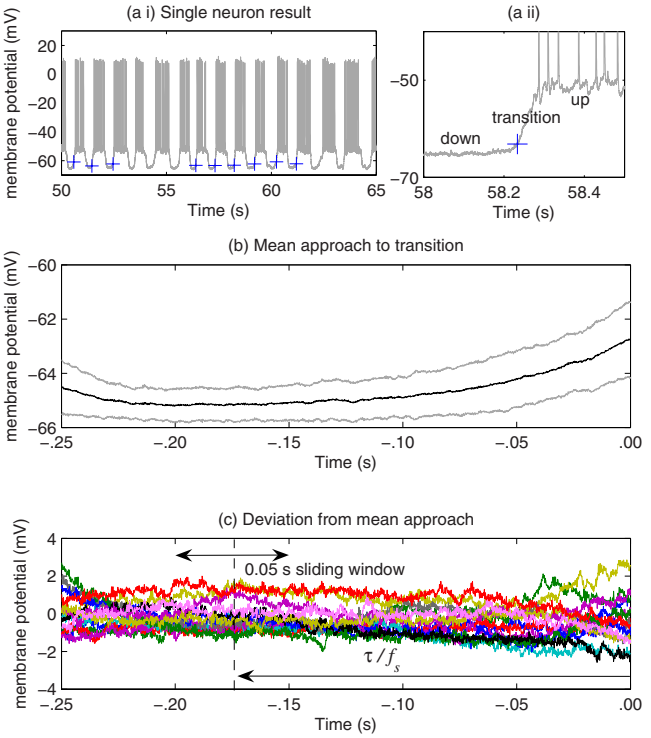

FIG. 3. (Color online) (a) An example sequence of membrane potential against time. For clarity, only 15 s out of 90 s has been shown. The points that have been identified as transitions are marked by crosses. A close-up view of one of the transitions is shown. (b) The mean membrane potential during the 0.25 s period before a transition, for the neuron shown in sequence (a). The average has been taken over all the identified transition periods. The x axis indicates time before transition—i.e., $t=0$ s denotes the transition point and $t=-0.25$ s denotes 0.25 s before the transition; the minus sign is introduced to enable the graph to be read left to right. The gray lines indicate one standard deviation either side of the mean. (c) The membrane potential minus the mean membrane potential, for the 0.25 s periods before some of the transitions. (For clarity, not all the series are shown.) Note how there is a wider spread in the sequences at the transition point ($t=0$) compared to 0.1 s previously ($t=-0.1$ s). The top arrow signifies the length of the sliding window that has been used to analyze the frequency data; the bottom arrow shows the time before the transition.

quency fluctuations and therefore such an approach restricts the frequency range that we can analyze.

The fact that the mean (i.e., the trend) $\bar{y}^k$ has been constructed from the transition segments $\tilde{y}^{ki}$ implies that this definition of fluctuation $\Delta\tilde{y}^{ki}$ is biased. (For example, if there were just one transition in the sequence then $\Delta\tilde{y}^{ki}$ would be identically zero.) For this reason we eliminate sequences that show less than 10 identifiable transitions.

For each of the detrended 0.25 s segments [i.e., each series of Fig. 3(c)] we construct the temporal power spectrum as a function of the time before the transition. We do this by taking a sliding 0.05 s long windows of data, and evaluating the Fourier transform of the detrended membrane potential within this window. Since the sample rate for the data is 10^4 Hz, there are 500 samples in each 0.05 s window. Figure 3(c) indicates how this is done.

Mathematically, we write

$$z^{ki}(j,\tau) = \Delta\tilde{y}^{ki}(Q - \tau - L/2 - 1 + j), \tag{3.6}$$

where $j=1,\ldots,L+1$ (where $L=0.05\ \text{s}\times f_s=500$ and indicates the length of the sliding window). The discrete index τ indicates the midpoint of the sliding window—the time before the transition t is given by τ/f_s. For $\tau<L/2$ and $\tau\geq Q-L/2$, we leave $z^{ki}(j,\tau)$ undefined. (Note on the plots we present time as negative so that increasing time, i.e., *decreasing* time before transition, can be read left to right.) Then, we define the discrete Fourier spectrum by taking a discrete Fourier transform

$$Z^{ki}(r,\tau) = \mathcal{F}[z^{ki}(j,\tau)], \tag{3.7}$$

where $\mathcal{F}$ is the discrete Fourier transform over index j and r is a discrete index that describes frequency. [Frequency $=r/(0.05\ \text{s})$, denoted by f_r, where $r=1,\ldots,Q$.]

We use a rectangular window rather than the more usual tapered window for the analysis because we wish to identify small variations in power at low frequencies on approach to the transition—i.e., we exploit the frequency resolution that a rectangular window gives. The disadvantage of this is spectral leakage, in this case the power spectrum at high frequencies can be contaminated by artifacts due to low frequency signals.

For each sequence, we then average the Fourier power spectrum over all the P^k segments preceding the identified transitions, to obtain an averaged spectrum $S^k(r,\tau)$ of temporal fluctuations as a function of time before transition,

$$S^k(r,\tau) = \frac{1}{P^k}\sum_{i=1}^{P^k} |Z^{ki}(r,\tau)|^2. \tag{3.8}$$

For one sequence, Fig. 4(a) shows such spectra for five of the 0.05 s windows (i.e., five τ values); the centers of the windows are at times of 25 ms, 50 ms, 75 ms, 100 ms, and 125 ms before the transition. Above about 500 Hz the spectra typically show white noise, but below this frequency there is a clear increase in power as frequency decreases. Moreover, when we look at the very low frequencies (long time scales), we can clearly see that the window closest to transition has the largest power. For this neuron there are resonances at about 140 Hz and 350 Hz. No other neuron showed clear indications of these resonances, and their origin has not been identified. We do not discuss them further here.

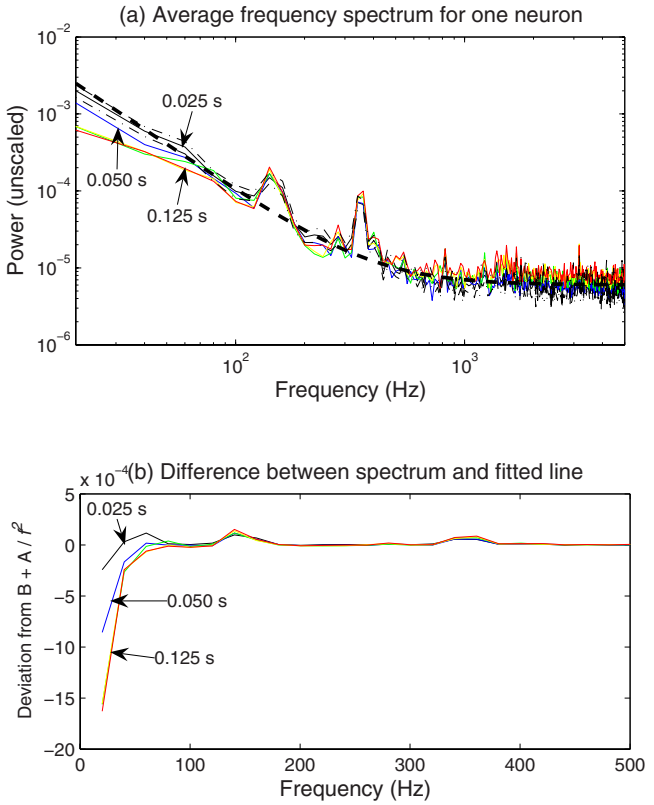

FIG. 4. (Color online) (a) A plot of the power spectrum for one neuron. The five lines denote the mean power over 0.050 s segments that are centred at 0.025 s (black), 0.050 s (blue), 0.075 s (green), 0.100 s (red), and 0.125 s (yellow) before the transition. The mean is taken over all the identified transitions in the sequence for this neuron. The dashed lines either side of the 0.025 s line indicate the standard uncertainty in this result. (The standard uncertainties for the other lines are similar in size.) Also shown by the heavy dashed line is a curve of the form $S(f)=B+A/f^2$, where S is power, f is frequency, and A and B are constants fitted by eye. (b) The power spectrum minus $S(f)$, for the neuron of part (a). Here we see the increase in power at low frequencies as the transition is approached.

In order to condense our results into a simply presentable form, we quantify the fluctuations in two ways. First, we quantify the size of the fluctuations by constructing the mean power $\bar{u}(\tau)$ as a function of the time before the transition—i.e., for each window we take the total power in the Fourier spectrum up to 500 Hz and we average over all the transitions in all the sequences (weighting each transition equally—i.e., each sequence is weighted by the number of transitions it contains),

$$\bar{u}(\tau) = \frac{\sum_{k=1}^{M} P^k u^k(\tau)}{\sum_{k=1}^{M} P^k} \tag{3.9}$$

where

$$u^k(\tau) = \sum_{r=1}^{25} S^k(r,\tau). \tag{3.10}$$

The "25" upper limit corresponds to the number of frequency steps that are contained below 500 Hz (=500 Hz × 0.05 s). Secondly, we quantify the time scale for the fluctuations by constructing the centroid of the frequency spectrum $\bar{c}(\tau)$ as a function of the time before the transition. Again, we average over all transitions in all sequences,

$$\bar{c}(\tau) = \frac{\sum_{k=1}^{M} P^k c^k(\tau)}{\sum_{k=1}^{M} P^k}, \tag{3.11}$$

where

$$c^k(\tau) = \frac{\sum_{r=1}^{25} f_r S^k(r,\tau)}{\sum_{r=1}^{25} S^k(r,\tau)}. \tag{3.12}$$

In these analyses we remove the spectrum for frequencies above 500 Hz on the grounds that this is dominated by white noise.

IV. RESULTS

The resulting plots are shown in Fig. 5. The horizontal axis shows the time before the transition—the zero point on the axis corresponds to the transition, and the vertical axes show how the power [Fig. 5(b)] and centroid [Fig. 5(c)] change as the transition is approached. Figure 5(a) shows the mean membrane potential, for comparison (each sequence being weighted by the number of transitions it contains.) It is clear from these figures that the power and centroid frequency are strongly correlated with the mean membrane potential. Specifically, as the membrane potential increases on the approach to a transition, the power in the fluctuations increases, and the centroid frequency decreases from about 110 Hz to 90 Hz (i.e., power increases and shifts to lower frequencies). This is what we would expect from the phase transition model. At earlier times, before about 0.15 s before the transition, the overall power reduces with increasing time, and the centroid frequency increases. This we attribute to the influence of the previous transition from an up to a down state. We have also repeated the calculations with a cutoff in the spectrum at 400 Hz—the results are similar, suggesting that the exact choice of cutoff is not particularly important. Use of a tapered Hann window rather than the rectangular window for weighting the sequences $z^{ki}(j,\tau)$ produces similar results (an increase in power and decrease in frequency as the transition is approached), but the uncertainties are larger. The analysis was also repeated separately for layer 3 and layer 5 neurons, but no qualitative difference in the trends was found; hence the results are presented together.

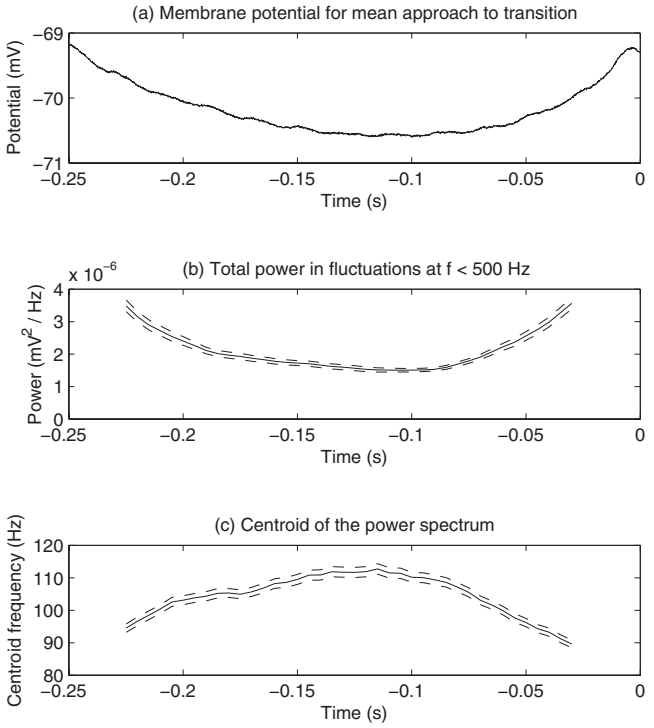

FIG. 5. (a) The mean membrane potential in the 0.25 s period before a down to up transition, averaged over all transitions used in this study, i.e., $\Sigma_{k=1}^{M} P^k \bar{y}^k(j) / \Sigma_{k=1}^{M} P^k$. Note that it rises on the approach to transition ($t=0$). Negative times denote the time before transition. (b) The mean fluctuation power as a function of time before transition. Note that only frequencies below 500 Hz have been used in this calculation. Averages have been taken over all sequences and transitions. The dashed lines indicate the standard uncertainty in the mean. (c) The centroid frequency of the power spectrum, averaged over all sequences used in this study, as a function of time before transition. The dashed lines indicate the standard uncertainty in the mean.

We now address the question of how much the spectrum of Fig. 4(a) (and the results of Fig. 5) can be attributed to the fact that the subtraction of the mean membrane potential still can leave a noticeable drift in the data sequence. Figure 3(c) shows that the spread of the detrended sequences increases as the transition is approached—i.e., the detrending has not been completely successful. Consider the example of a linear drift—i.e., a function of form $y(t)=at+b$ $(0<t<T)$, where t is time and a and b are constants, repeating every time T in a sawtooth fashion. If we were to take the Fourier transform of such a function we would produce a power spectrum S that had form $S(f) \sim 1/f^2$; this would manifest itself as a line of gradient −2 on a log-log plot such as Fig. 4(a). On Fig. 4(a) we have superposed a curve of the form $S(f)=B+A/f^2$; the "A" constant accounts for the white-noise spectrum at high frequencies.

Although Fig. 4(a) does have a section that has a gradient close to −2, it is clear that not all of the shape can be attributed to this effect. In particular, at low frequencies (below about 100 Hz), we can clearly identify that as the transition is approached, the power at the very lowest frequencies increases more rapidly than that at higher frequencies. We show this in Fig. 4(b) where we plot power minus the trend

line $B+A/f^2$, against frequency; at low frequencies the power clearly increases as the transition is approached. This effect is demonstrated in the centroid plot of Fig. 5(c). If the results were purely driven by this artifact, we would expect the centroid not to change, since the power S at all frequencies would grow proportionally according to $S(f)=A/f^2$, where A is a constant (when evaluating the centroid, we only consider frequencies up to 500 Hz, since white noise appears to dominate from then on).

Therefore, we suggest that the results do show some evidence of an increase in fluctuation power, and a decrease in fluctuation frequency (that is, an increase in fluctuation time scale) as the transition is approached.

V. CONCLUSIONS

In this work we have attempted to quantify the magnitude of power fluctuations and time scales as a transition is approached between the down and up state of a cortical neuron during slow-wave sleep. We find that increases in both these are broadly consistent with critical slowing, providing some evidence to support the assertion that transitions between these cortical states can be described by first-order phase transitions.

The major limitations with this analysis are the identification of the positions of the transitions, and the need to separate out fluctuations in membrane potential from trends in the mean membrane potential. The latter is particularly troublesome; given that the predicted shift in power towards low frequencies, and that a trend is simply a very low-frequency response, it is unclear whether such a separation is strictly possible. However, we believe that the qualitative trends shown in this paper are still valid.

Ideally, we would wish to look at spatial correlation functions. However, such data are not readily obtainable at the present time. If, in the future, high-quality many-electrode intracellular voltages can be obtained, an analysis of the spatial statistics on the approach to transition would be very worthwhile.

[1] M. Steriade, A. Núnez, and F. Amzica, J. Neurosci. **13**, 3252 (1993).
[2] M. Steriade, I. Timofeev, and F. Grenier, J. Neurophysiol. **85**, 1969 (2001).
[3] G. Tononi and C. Cirelli, Sleep Med. Rev. **10**, 49 (2006).
[4] D. M. Rector, I. A. Topchiy, K. M. Carter, and M. J. Rojas, Brain Res. **1047**, 45 (2005).
[5] M. Massimini, R. Huber, F. Ferrarelli, S. Hill, and G. Tononi, J. Neurosci. **24**, 6862 (2004).
[6] M. Volgushev, S. Chauvette, M. Mukovski, and I. Timofeev, J. Neurosci. **26**, 5665 (2006).
[7] P. L. Nunez, Math. Biosci. **21**, 279 (1974).
[8] W. J. Freeman, in *Induced Rhythms of the Brain*, edited by E. Basar and T. H. Bullock (Birkhaeuser, Boston, 1992), Chap. 9, pp. 183–199.
[9] V. K. Jirsa and H. Haken, Phys. Rev. Lett. **77**, 960 (1996).
[10] M. L. Steyn-Ross, D. A. Steyn-Ross, J. W. Sleigh, and D. T. J. Liley, Phys. Rev. E **60**, 7299 (1999).
[11] M. T. Wilson, D. A. Steyn-Ross, J. W. Sleigh, M. L. Steyn-Ross, L. C. Wilcocks, and I. P. Gillies, J. Comput. Neurosci. **21**, 243 (2006).
[12] I. Bojak and D. T. J. Liley, Phys. Rev. E **71**, 041902 (2005).
[13] P. A. Robinson, C. J. Rennie, J. J. Wright, and P. D. Bourke, Phys. Rev. E **58**, 3557 (1998).
[14] C. J. Rennie, J. J. Wright, and P. A. Robinson, J. Theor. Biol. **205**, 17 (2000).
[15] P. A. Robinson, C. J. Rennie, and D. L. Rowe, Phys. Rev. E **65**, 041924 (2002).
[16] B. Molaee-Ardekani, L. Senhadji, M. B. Shamsollahi, B. Vosoughi-Vahdat, and E. Wodey, Phys. Rev. E **76**, 041911 (2007).
[17] M. T. Wilson, M. L. Steyn-Ross, D. A. Steyn-Ross, and J. W. Sleigh, Phys. Rev. E **72**, 051910 (2005).
[18] D. A. Steyn-Ross, M. L. Steyn-Ross, M. T. Wilson, and J. W. Sleigh, Phys. Rev. E **74**, 051920 (2006).
[19] Y. Chagnac-Amitai, H. J. Luhmann, and D. A. Prince, J. Comp. Neurol. **296**, 598 (1990).
[20] M. Steriade, Neuroscience **101**, 243 (2000).
[21] K. D. Games and J. A. Winer, Hear. Res. **34**, 1 (1988).
[22] M. Brecht, A. Krauss, S. Muhammed, L. Sinai-Esfahani, S. Bellanca, and T. W. Margrie, J. Comp. Neurol. **479**, 360 (2004).
[23] J. N. J. Reynolds, B. I. Hyland, and J. R. Wickens, J. Neurosci. **24**, 9870 (2004).